crystals

MDPI

Article

The Study of High Breakdown Voltage Vertical GaN-on-GaN *p-i-n* Diode with Modified Mesa Structure

Wen-Chieh Ho [1], Yao-Hsing Liu [1], Wen-Hsuan Wu [1], Sung-Wen Huang Chen [1], Jerry Tzou [2], Hao-Chung Kuo [1,*] and Chia-Wei Sun [1]

[1] Department of Photonics and Institute of Electro-Optical Engineering, National Chiao Tung University, 1001 Ta Hsueh Road, Hsinchu 30010, Taiwan; jerryho.eo07g@nctu.edu.tw (W.-C.H.); yawshine@gmail.com (Y.-H.L.); alexwu8591@gmail.com (W.-H.W.); wenisbest@hotmail.com (S.-W.H.C.); chiaweisun@nctu.edu.tw (C.-W.S.)

[2] Taiwan Semiconductor Research Institute (TSRI), Hsinchu 30078, Taiwan; ajtzou@narlabs.org.tw

* Correspondence: hckuo@faculty.nctu.edu.tw; Tel.: +886-3-571-2121 (ext. 56333)

Received: 29 June 2020; Accepted: 12 August 2020; Published: 18 August 2020

check for updates

Abstract: In this paper, we fabricated Gallium Nitride (GaN) vertical *p-i-n* diodes grown on free-standing GaN (FS-GaN) substrates. This homogeneous epitaxy led to thicker GaN epi-layers grown on the FS-GaN substrate, but a high crystalline quality was maintained. The vertical GaN *p-i-n* diode showed a low specific on-resistance of 0.85 mΩ-cm^2 and high breakdown voltage (BV) of 2.98 kV. The high breakdown voltage can be attributed to the thick GaN epi-layer and corresponds to the mesa structure. Improvement of the device characteristics by the mesa structure was investigated using device simulations. We proved that a deeper mesa depth is able to decrease the electric field at the bottom of the mesa structure. Furthermore, a smaller mesa bevel angle will assist the BV up to 2.98 kV at a 60° bevel angle. Our approach demonstrates structural optimization of GaN vertical *p-i-n* diodes is useful to improve the device performance.

Keywords: Gallium Nitride (GaN); vertical *p-i-n* diodes; FS-GaN substrate; vertical diode

1. Introduction

Gallium Nitride (GaN)-based power devices have attracted much attention due to their excellent properties, such as their high breakdown electric field (~3.3 MV/cm), high power switching efficiency, and high thermal stability [1,2]. In addition, inherent polarization is built in the AlGaN/GaN hetero-junction structure, leading to a high sheet carrier density (n_s) in the two-dimensional electron gas (2DEG) as well as a decrease in the on-state resistance (R_{on}) for power switching applications. As compared to lateral GaN-based devices, vertical GaN-based devices are capable of handling a larger current with a given device footprint. Typical vertical GaN-based power devices are grown on free-standing GaN substrates. The homogeneous epitaxy is capable of reducing the threading dislocation down to ~10^4–10^5 cm^{-2}, leading to a remarkable improvement in the performance of vertical GaN *p-i-n* diodes and Schottky barrier diodes (SBDs) [3].

In previous studies, vertical GaN-on-GaN *p-i-n* diodes with a breakdown voltage (BV) at 4700 V have been fabricated by using multiple Si-doped GaN drift layers to reduce the peak electrical field of the *p-n* interface [4]. Moreover, the GaN-on-GaN *p-i-n* diode had a low R_{on} of ~1.25 mΩ-cm^2, and the Baliga's figure-of-merit (BFOM) of ~10 GW/cm^2 was also obtained by the high-level injection and photon recycling effect [5]. The BV of a vertical GaN-on-GaN *p-i-n* diode can be enhanced through electrical field modulation by using various termination techniques such as the metal field plate structure [6] and multi-step mesa structure formed by reactive ion etching (RIE) [7]. Another BV improvement method considers the drift region length. In conventional Si-based *p-n* diodes, a longer drift length may effectively reduce the peak electric field, as shown in Figure 1. When a power diode is under reverse bias conditions, the reverse voltage is supported by the depletion region formed by the p^+-n^- junction. In the depletion region, the number of ionized atoms in the p^+-region should be equal to those in the n^--region. However, the depletion region almost extends into the n^--drift region because the donor concentration (N_D) is much higher than the accepter concentration (N_A). In the non-punch-through case, the distribution of the electric field is a triangle, and it decreases to zero at the boundary voltage in the standing region. Hence, we can enhance the BV by extending the drift length, which means the BV can be improved by increasing the n^--region thickness.

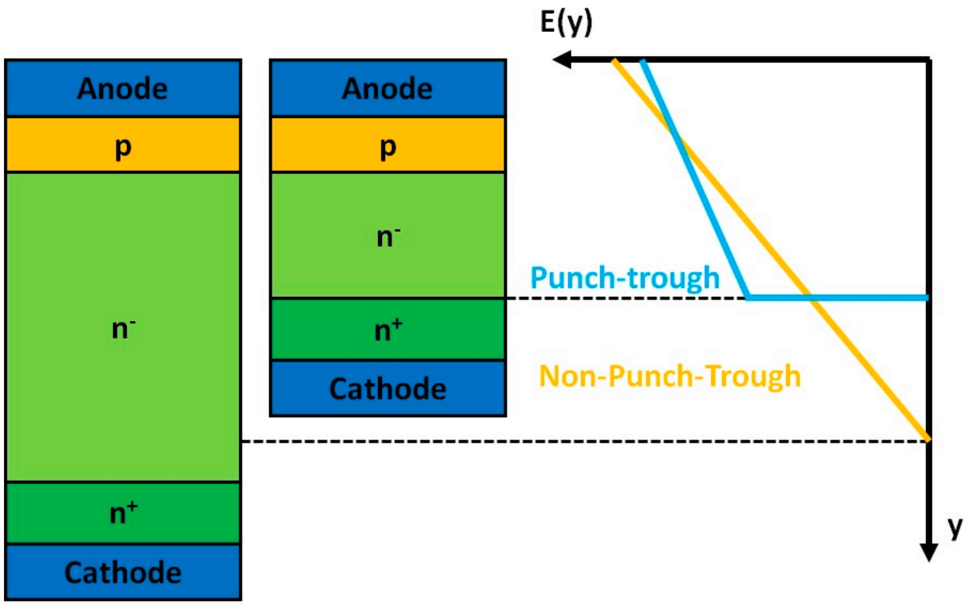

Figure 1. Schematic structure of *p-n* junctions in non-punch-through case and punch-through case, and the corresponding electric field profiles.

However, thicker epi-layers will result in increased strain from lattice mismatch or different thermal expansion coefficients. The GaN-on-GaN homogeneous epitaxy provides a way to overcome the high stress from thick epi-layers. Furthermore, thicker epi-layers require deeper mesa etching depths for device isolation. The etched profile of the deep mesa is crucial to improve the BV [8]. In this paper, we developed a 13-µm-thick n^--layer to improve the BV. A specific on-resistance of 0.75 mΩ·cm^2 for the vertical GaN *p-i-n* diode was achieved, and it had a BV of 2.98 kV. This device achieved a Baliga's figure-of-merit (BFOM) of 11.8 GW/cm^2. BV improvement was investigated using simulated models of vertical GaN *p-i-n* diodes. We found BV was affected by the n^--layer thickness and mesa structure. In addition, the simulation also suggests the mesa bevel angle impacts the BV. Raman spectroscopy, transmission electron microscopy (TEM), and X-ray diffraction (XRD) were employed to analyze the parameters of GaN grown on FS-GaN substrates.

2. Experimental Section

2.1. Device Fabrication

The GaN *p-i-n* diode structure was heterogeneously grown on a free-standing GaN substrate by metal organic chemical vapor deposition (MOCVD). The bulk GaN substrate was *n*-type with Ge doping and had a thickness of 350 µm. On the bulk GaN, 2-µm-thick n^+-GaN ([Si] = 2×10^{18} cm^{-3}), 13-µm-thick n^--GaN drift ([Si] = 1.2×10^{16} cm^{-3}), 400-nm-thick p^+-GaN ([Mg] = 6.5×10^{16} cm^{-3}), and 30-nm-thick p^{++}-GaN ([Mg] = 2×10^{18} cm^{-3}) layers were grown, respectively. The epi-wafers were separated into 2×2 cm^2 pieces. The *p-i-n* diode process started with deposited back ohmic contact.

A specific contact resistance (ρ_c) of 3.75×10^{-4} Ω-cm^2 was obtained by Ti/Al (25/125) and thermal metallization by rapid thermal annealing (RTA) at 550 °C for 90 s. Next, the deep mesa was etched by Cl_2/BCl_3-based dry-etching. Based on this epitaxial structure, we fabricated different diodes including planar and mesa types with 400 µm width and 14 µm depth.

Afterwards, the oxygen-based plasma pre-treatment oxidized the surface to form the native GaO_x compounds. GaO_x was subsequently removed by 1:1 HCl solution, and then the *p*-GaN ohmic contact metal was deposited by Ti/Al (50/300 nm). To improve the BV, we also set the field plate at the sidewall of the mesa, which was 50 µm wider than the mesa. The stacking insulator layers included SOG and 1-µm-thick SiO_2. The thickness of SOG was equal to the mesa etching depth. Next, the Ti/Au (25/300 nm) pad metal was deposited on the pad region after the contact vias were etched. The device structure is shown in Figure 2.

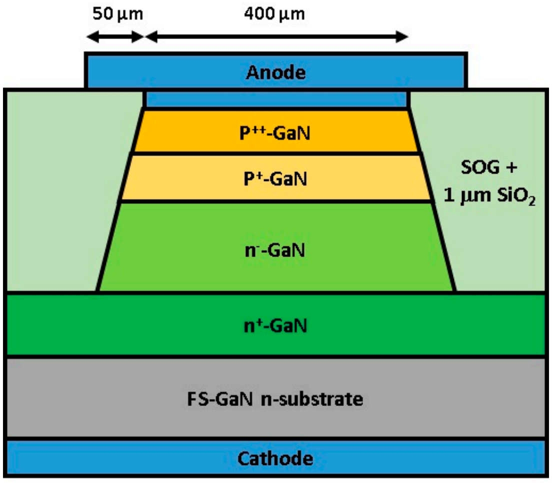

Figure 2. The schematic epitaxy structure of a vertical GaN *p-i-n* diode.

2.2. Device Simulations

An avalanche breakdown essentially results from the impact ionization process being dominated by electrons and holes, and this impacts the ionization coefficients. In the case of p-n junctions, an avalanche breakdown occurs when the impact ionization integral reaches the following condition:

$$\mathrm{I_n} = \int \alpha_\mathrm{n} \exp\left(\int^{\mathrm{W}} \alpha_\mathrm{p} - \alpha_\mathrm{n} \mathrm{dv}\right)/\mathrm{dw} = 1 \tag{1}$$

where $\mathrm{I_n}$ is the impact ionization integral of electrons, and $\alpha_\mathrm{n} = a_\mathrm{n} \times \exp(-b_\mathrm{n}/\mathrm{E})$ and $\alpha_\mathrm{p} = a_\mathrm{p}\ \exp(-b_\mathrm{p}/\mathrm{E})$ are the impact ionization rates of electrons and holes, respectively. Accordingly, a precise model for the breakdown and the subsequent characteristics of power devices are based on accurate impact ionization coefficients. The impact ionization coefficients are generally obtained from Monte Carlo methods or experiments. However, different physical mechanisms or calculation methods will result in different values, and different fabrication processes or structures will also lead to various experimental values.

Several different impact ionization coefficients are compared with the APSYS simulation, and the conclusion is that the impact ionization coefficient from Baliga [9] had the closest fit to the simulation and experimental breakdown voltage results. The impact ionization coefficients for electrons and holes from Baliga are functions of an inverse electric field and are shown below.

$$\alpha_n = 1.5 \times 10^5 \mathrm{cm}^{-1} \times \exp\left(\frac{-1.41 \times 10^7 \mathrm{V/cm}}{E}\right) \tag{2}$$

$$\alpha_p = 6.4 \times 10^5 \mathrm{cm}^{-1} \times \exp\left(\frac{-1.46 \times 10^7 \mathrm{V/cm}}{E}\right) \tag{3}$$

The growth technique for GaN and orientation of the epitaxial layer lead to various values of material parameters. Vertical GaN devices are grown on a free-standing GaN substrate in a Wurtzite crystal structure along the c-axis of the crystal by MOCVD. The fundamental material parameters according to a MOCVD-grown epitaxial layer along the c-axis on a Wurtzite crystal structure are used in this thesis, and these are listed in Table 1.

Table 1. Material parameters of Wurtzite GaN.

Material Parameters	Values
Lattice constant (Å)	a = 3.192 c = 5.185 [10]
Dielectric constant	8.9 [11]
Electron affinity (eV)	4.5 [11]
Effective electron mass (m_0)	0.2 [12]
Conduction band density of state N_c (cm^{-3})	2.3×10^{18} [12]
Effective hole mass (m_0)	1.25 [13]
Valence band density of state N_v (cm^{-3})	3.5×10^{19} [12]
Critical breakdown field (MV/cm)	3.5 [11]

To build an accurate simulation model, several physical phenomena also need to be prudently considered. We collected several crucial physical models and model parameters, including the impact ionization coefficients we mentioned before; they are listed in Table 2, and they are used in the simulation of this thesis.

In this paper, we investigated BV improvement by different mesa depths and bevel angles through simulations. The simulated mesa depth was modified from 0 to 14 µm. The bevel mesa angle in every model was different, with values of 60, 70, 80, and 90 degrees.

Table 2. The physical models and model parameters.

Physical Phenomenon	Models	Parameters	Values
Bandgap	Temperature dependent bandgap model (@0K)	Reference bandgap (E_{g0})	3.53 eV [14]
		Reference electron affinity (Chi_0)	4.1 eV [11]
		Alpha	9.09×10^{-4} eV/K
		Beta	830 K
Incomplete ionization	Silicon (n-doped) [15]	Donor activation energy (ΔE_D)	17 meV [15]
		Constant (α_n)	3.4×10^{-9} eV-cm [16]
	Magnesium (p-doped) [17]	Acceptor activation energy (ΔE_D)	240 meV
		Constant (α_p)	3.14×10^{-8} eV-cm [17]
Bandgap narrowing	Jain-Roulston [16]	Constant (K)	1.15×10^{-8} eV-cm [16]
Polarization	Spontaneous polarization [18]	Spontaneous Polarization (Psp)	−0.029 C/m [18]
	Piezo-electric polarization [19]	Elastic constant (c_{13})	68 GPa [19]
		Elastic constant (c_{33})	354 GPa [19]
		Piezoelectric coefficient(e_{31})	−0.34 C/m^2 [19]
		Piezoelectric coefficient(e_{33})	0.62 C/m^2 [19]
		relax	1

Table 2. *Cont.*

Physical Phenomenon	Models	Parameters	Values
Electron mobility	Low field doping-dependent Arora Model [20]	μ_{min}	115 cm^2/V-s
		μ_{max}	1800 cm^2/V-s
		α	0.8
		Reference doping (N_{ref})	7×10^{16} cm^{-3}
		β_1	−1.5
		β_2	−1.5
		β_3	3.02 [20]
		β_4	0.81 [20]
	High field transferred electron effect model [21]	E_c	1.7×10^5 V-cm [21]
		n_1	4.19 [21]
		n_2	0.885 [21]
		a	5.64
Hole mobility	Low field doping-dependent Arora Model [22]	μ_{min}	12 cm^2/V-s
		μ_{max}	167 cm^2/V-s
		α	2.0 [22]
		Reference doping (N_{ref})	3×10^{17} cm^{-3}
		β_1	2.0
		β_2	−2.34
		β_3	0.869
		β_4	−2.311
	High field Caughey Thomas model	μ_{h0}	70 cm^2/V-s
		Saturation velocity ($v_{h,sat}$)	7×10^6 cm-s^{-1}
		β	0.725
Impact ionization	Electron impact ionization Coefficients [9]	a_n	1.5×10^5 cm^{-1} [4.3]
		b_n	1.41×10^7 V-cm^{-1} [9]
	Hole impact ionization Coefficients [9]	a_p	6.4×10^5 cm^{-1} [9]
		b_p	1.46×10^7 V-cm^{-1} [9]
Radiative recombination	Radiative recombination constant	C_{rad}	1.1×10^{-10} cm^3-s^{-1} [23]
SRH recombination	Constant lifetime	Electron lifetime (τ_n)	0.7×10^{-9} s
		Hole lifetime (τ_p)	2×10^{-9} s
Auger recombination	Electron coefficient [24]	A_n	3×10^{-31} cm^6-s^{-1} [24]
	Hole coefficient [24]	A_p	3×10^{-31} cm^6-s^{-1} [24]

3. Results and Discussion

Figure 3 shows the growth parameters of GaN grown on a FS-GaN substrate. As we can see from Figure 3a, the TEM image shows few threading dislocations (TDs) can be observed in the 15 µm MOCVD-grown GaN epi-layer regions. The threading dislocation density (TDD) can be estimated to about 3×10^6 cm^{-2} for 15-µm-thick GaN epilayers. The extremely low TDD can be attributed to the better crystalline quality of thick GaN epilayers and less residual strain caused by gradual strain relaxation due to the homogeneous epitaxy. To analyze the residual strain in the GaN epilayers, Raman backscattering measurements were performed at room temperature. Figure 3b shows the

Raman spectrum for a 15-µm-thick GaN epitaxial layer grown on a GaN substrate. The Raman shift peak of the $E_{2(\mathrm{high})}$ mode was located at around 567.6 cm^{-1}. Accordingly, the in-plane compressive stress σ for the GaN epitaxial layer was estimated to 0.22 GPa, with the presence of thicker GaN epilayer, by using the following equation [25]:

$$\Delta\omega_{E_2} = \omega_{E_2} - \omega_0 = C\sigma \tag{4}$$

where $\Delta\omega$ is the Raman peak shift (0.189 cm^{-1}) difference between the strained GaN epitaxial layer ω_{E2} and the unstrained GaN epitaxial layer ω_0 (566.5 cm^{-1}). C is the biaxial strain coefficient, which is 2.25 cm^{-1}/GPa [26]. The X-ray diffraction (XRD) rocking curves are shown in Figure 3c. The linewidths for (002) and (102) planes are 67 and 135 arcsec, respectively. The XRD linewidths for (102) and (002) planes are related to the edge and screw threading dislocation densities, respectively [27]. The narrow linewidth indicates improved GaN crystalline quality. These results indicated that the quality of 15-µm-thick GaN grown on the FS-GaN substrate was excellent.

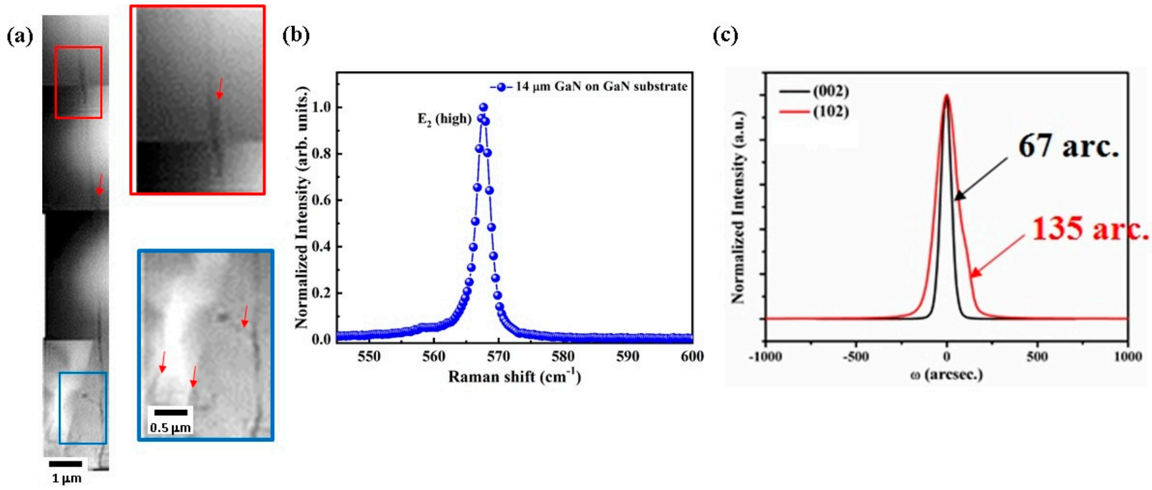

Figure 3. (**a**) TEM image of 15-µm-thick GaN epilayers grown on the FS-GaN substrate. The red arrows indicate the TDs. The diffraction condition is g = 0002. (**b**) Raman spectrum of a thick GaN epitaxial layer. (**c**) XRD rocking curves of a thick GaN epitaxial layer, and the (002) and (102) planes are shown.

Figure 4a shows the measured GaN *p-i-n* diode forward currents as a function of forward bias. The turn-on voltages (V_F) for the *p-i-n* diodes were 1.2 and 1.4 V for planar and mesa-type *p-i-n* diodes, respectively. The turn-on voltage was defined at the current density of 1 mA/cm^2. The specific on-resistances ($R_{\mathrm{on,sp}}$) can be calculated as 1.27 and 0.84 mΩ-cm^2 for planar and mesa-type *p-i-n* diodes, respectively. Figure 4b shows the reverse I–V characteristics of GaN *p-i-n* diodes. Reverse leakage of the planar diode was slightly increased compared to the mesa-type *p-i-n* diode. The ideal factor is 1.9, which was obtained from the forward bias region. The ideal factor values deviated from the ideal value of 1. Ideally, electrons and holes are recombined through the band-to-band transition in the active region. However, in real applications, the *p-i-n* diode usually undergoes a Shockley–Read recombination (SRH), in which electron–hole recombination occurs through a localized state or deep traps, resulting in a large value for the ideal factor [24].

Figure 5 shows the BVs of planar and mesa-type *p-i-n* diodes, respectively. The BV increased from 2000 to 2981 V due to the mesa-type *p-i-n* diode. The BV was defined with a reverse bias when the leakage reached 4 mA, which is the detection limit for the high-power device measurement system. A specific on-resistance of 0.84 mΩ·cm^2 was extracted using the active region from the mesa-type diode. With on-resistance and BV of 2.98 kV, this device achieved a Baliga's figure-of-merit (BFOM) of 10.5 GW/cm^2.

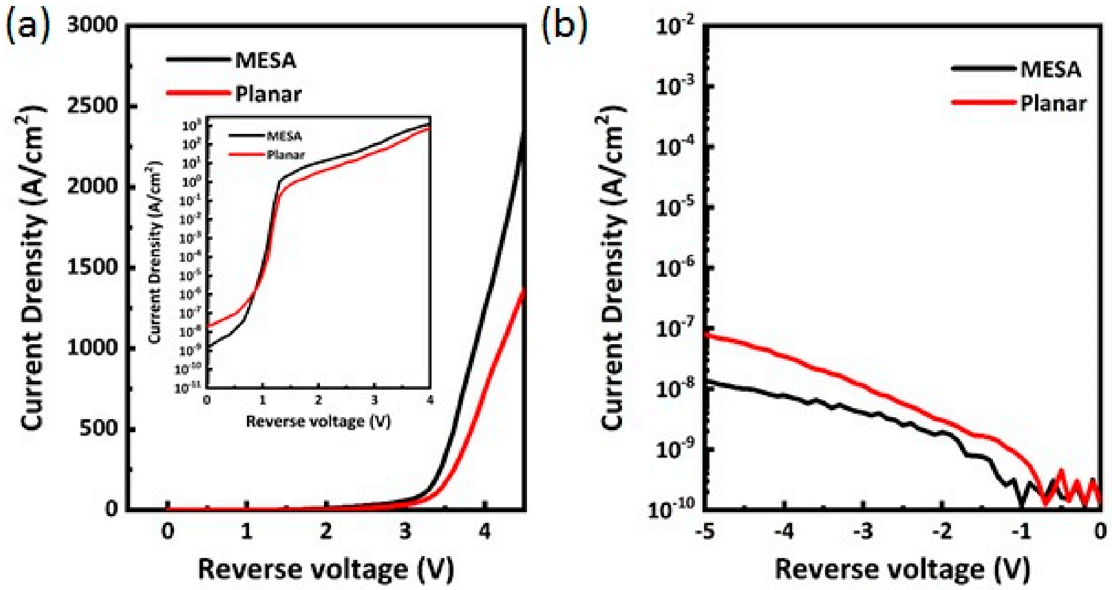

Figure 4. (**a**) Forward current and (**b**) reverse current as a function of bias. Forward current and specific on-resistance are normalized by the pad size. The inset of Figure 4a shows the forward I-V curves in a semilog scale.

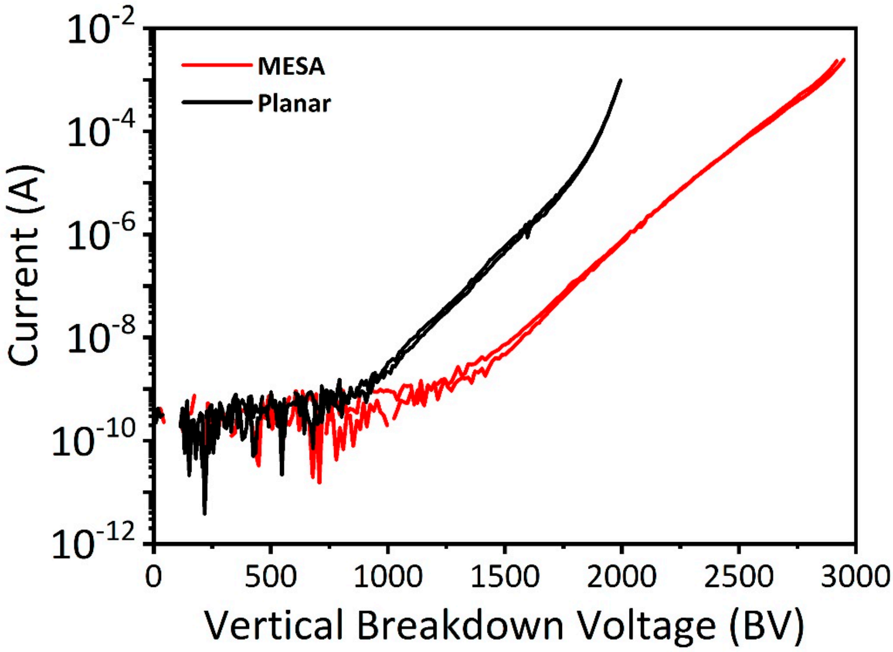

Figure 5. Reverse breakdown voltage measurement results of GaN *p-i-n* diodes with (red line) and without (black line) the mesa structure. The BV was defined as 4 mA. Each type of GaN *p-i-n* diode shows two I-V curves from two different diodes, respectively.

To understand how the mesa structure improved the BV, we carried out simulations using software by Crosslight APSYS to investigate the electric field distribution of *p-i-n* diodes. At first, we investigated the punch-through condition by simulating a planar *p-i-n* diode without a mesa structure. As shown in Figure 6, the electric field distribution is a trapezoid and the drift layer is fully depleted. Under the punch-through condition, the breakdown voltage was 2983 V, with a specific on-resistance of 0.39 mΩ-cm^2, and the maximum electric field was 3.45 MV/cm corresponding to the limit of the electric breakdown field of GaN. There was a difference between specific on-resistances in simulated results and experimental data, which can be attributed to the high contact resistance of ohmic contacts. The barrier height of the metal–semiconductor interface was set to 0 eV for the ideal case in our simulation. Nevertheless, our simulation fit our BV data, which means that the simulated electric field matched the real sample.

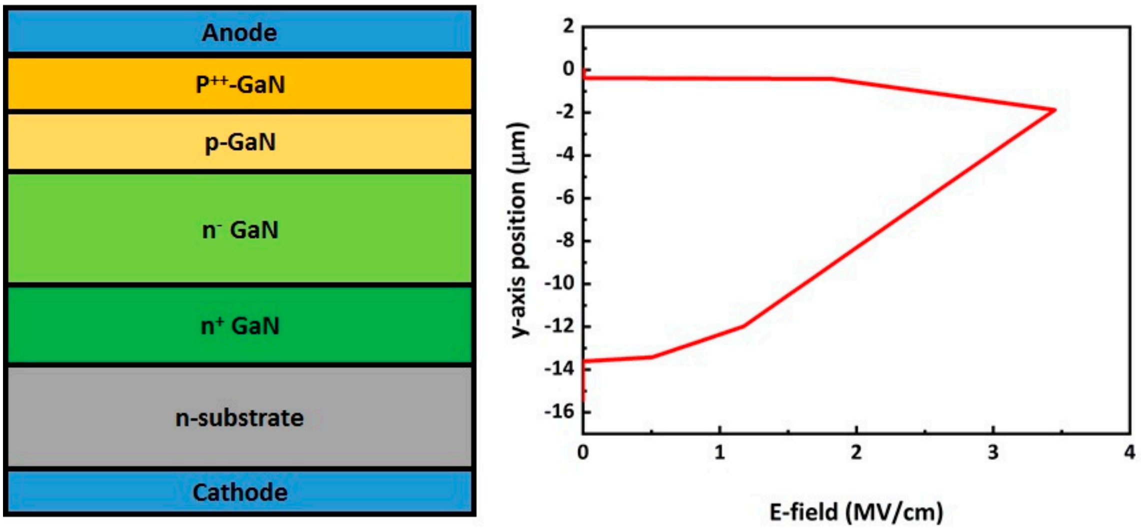

Figure 6. The electric profile along the midline for the planar model at a reverse bias of 2983 V.

Secondly, we simulated devices with field plates and different mesa depths. We investigated how the mesa depth affects the BV device characteristics. Figure 7 shows the electric field profiles of different devices at a reverse bias of 500 V. The strongest electric field was located at the bottom of the mesa, which was also the point where breakdown occurred. As can be seen, the BV was notably lower than the planar device when the mesa depth was lower than 8 μm. Afterwards, as we increased the mesa depth beyond 8 μm, the integration area of depletion was close to that of the planar device despite the breakdown still occurring at the bottom of the mesa. In other words, the breakdown voltage was close to the planar device for the diode with a mesa depth greater than 14 μm.

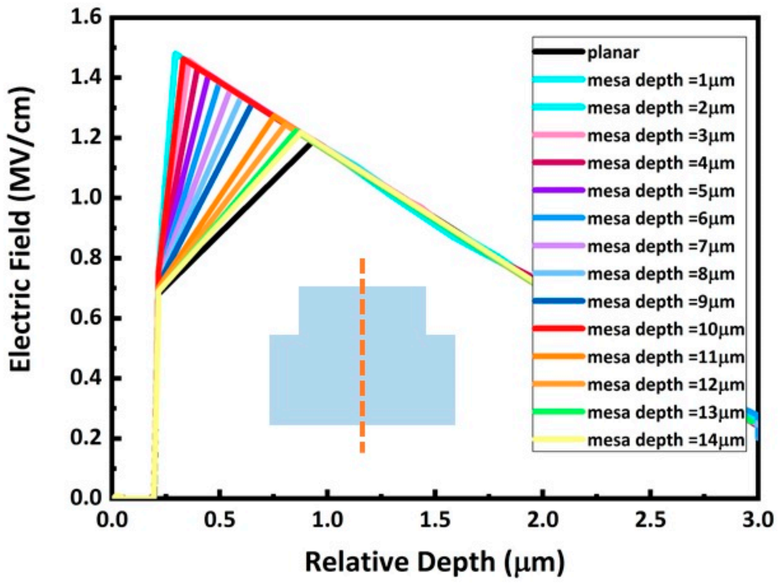

Figure 7. The electric field profile along the mesa midline for different devices at a reverse bias of 500 V.

Furthermore, the mesa bevel angle cannot be vertical to the horizon due to the ICP-RIE etching process. The bevel angle is also key in modifying the electric filed distribution for a *p*-*i*-*n* diode. Figure 8a shows the simulated peak electric field as a function of different mesa bevel angles. The mesa depth was less than 4 μm, taking the models with a depth of 2 μm, as shown in Figure 8a. The smaller the bevel angle, the stronger the electric field at the edge of the mesa was because the depletion region decreased from the lightly doping side to the highly doping side according to the epitaxial structure. As shown in Figure 8a, the electric field of the smaller bevel angle was higher than those of the more vertical ones, leading to a lower BV. In contrast, mesa depths greater than 4 μm are shown in the simulation in Figure 8b. When the mesa depth was 6 μm, we can see the BV was higher with a smaller bevel angle since the bevel edge provides a gradually distributed electric field. Figure 9 shows the electric field distribution contours of the 14-μm-deep mesa with different bevel angles. We note that the electric field is highly crowded at the bottom corners of the mesa structure, but it uniformly separated as we decreased the bevel angle. This is why we can enhance the BV by deep mesa etching.

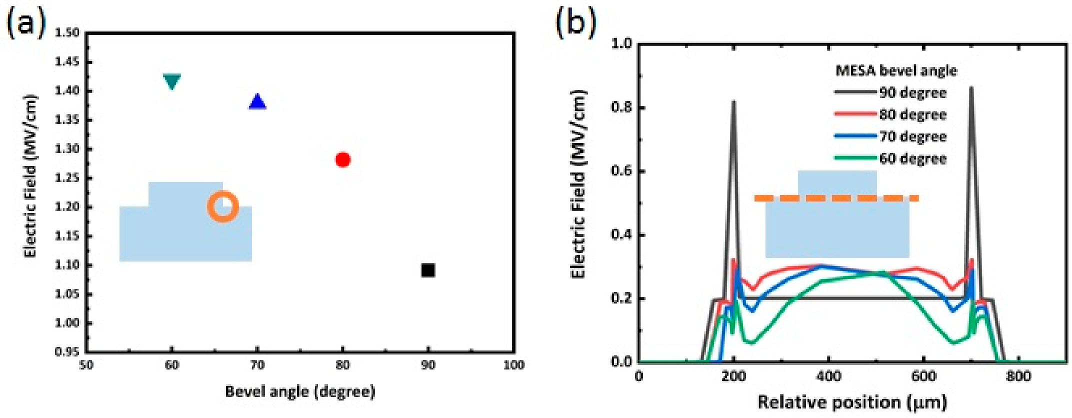

Figure 8. (**a**) Electric field magnitude at the bottom of a 2-μm mesa for different bevel angles at a reverse bias of 500 V. (**b**) Electric field distribution along the bottom of a 6-μm mesa for different bevel angles at a reverse bias of 500 V.

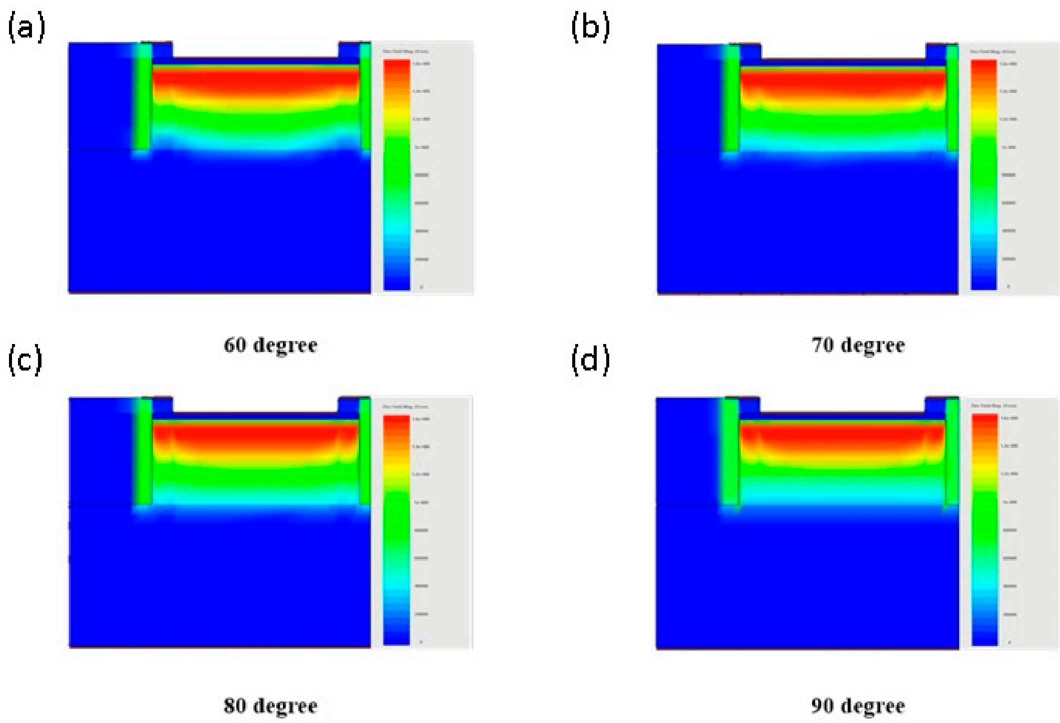

Figure 9. Simulated electric field distributions for GaN *p-i-n* diodes with different bevel angles: (**a**) 60°, (**b**) 70°, (**c**) 80°, and (**d**) 90°. The simulated reverse bias was 500 V.

Finally, we compared the device performance with the reported experimental devices. Here, we benchmark other previous reports of vertical GaN *p-i-n* diodes in Figure 10 [28–37]. A higher breakdown voltage was obtained by increasing the mesa depth and was closer to the material limit of GaN.

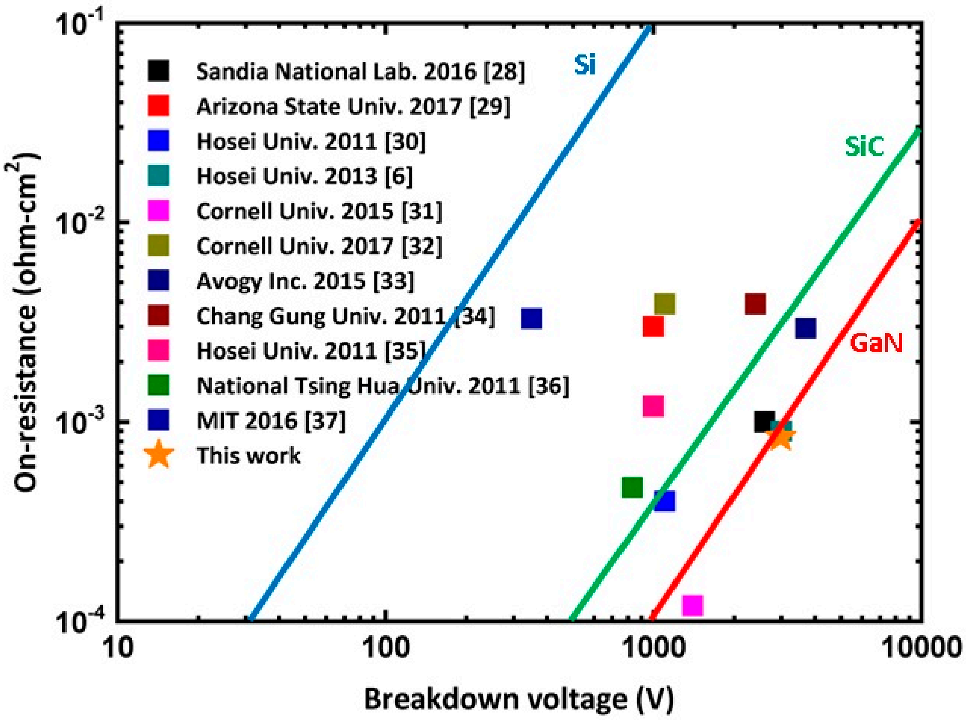

Figure 10. Benchmarks from other reports of vertical GaN *p-i-n* diodes [28–37].

4. Summary

We fabricated vertical GaN *p-i-n* diodes with a high BV using a 14-µm-thick GaN-on-GaN homogeneous epitaxy. The TEM showed a TDD of 10^6 cm^{-2}, and the Raman spectroscopy and XRD rocking curves showed the high quality and low strain for GaN epi-layers grown on a FS-GaN substrate. BV improvement was investigated by simulations, and the results suggest that the BV can be further improved using a mesa structure. Furthermore, we found that the breakdown voltage could be improved by increasing the mesa depth. A deep mesa structure provides a more gradual electric field distribution, and this affects the breakdown voltage more in the device with a greater mesa depth. Compared to the reported experiment, the strategy of increasing the mesa depth could improve the breakdown voltage of vertical GaN *p-i-n* diodes.

Author Contributions: W.-C.H., Y.-H.L., W.-H.W., S.-W.H.C., J.T., H.-C.K., and C.-W.S. discussed the topic. W.-C.H. fabricated the different devices and performed the measurements. All authors discussed the data analysis and interpretation, and contributed equally to the writing of the manuscript. All authors have read and agreed to the published version of the manuscript.

Funding: This study was funded by the Ministry of Science and Technology of Republic of China under grant number MOST 109-2218-E-182-001.

Conflicts of Interest: The authors declare no conflict of interest.

References

1. Mishra, U.K.; Parikh, P.; Wu, Y.F. AlGaN/GaN HEMTS: An overview of device operation and applications. *Proc. IEEE* **2002**, *90*, 1022–1031. [CrossRef]
2. Chow, T.P.; Tyagi, R. Wide bandgap compound semiconductors for superior highvoltage unipolar power devices. *IEEE Trans. Electron Devices* **1994**, *41*, 1481–1483. [CrossRef]

3. Liu, X.; Liu, Q.; Wang, J.; Yu, W.; Ao, J.P. 1.2 kV GaN Schottky barrier diodes on free-standing GaN wafer using a CMOS-compatible contact material. *Jpn. J. Appl. Phys.* **2017**, *56*, 026501. [CrossRef]
4. Ohta, H.; Nakamura, T.; Mishima, T. High quality free-standing GaN substrates and their application to high breakdown voltage GaN p-n diodes. In Proceedings of the 2016 IEEE International Meeting for Future of Electron Devices, San Francisco, CA, USA, 3–7 December 2016; pp. 23–26.
5. Nomoto, K.; Hu, Z.; Song, B.; Zhu, M.; Qi, M.; Yan, R.; Protasenko, V.; Imhoff, E.; Kuo, J.; Kaneda, N.; et al. GaN-on-GaN p-n power diodes with 3.48 kV and 0.95 mΩ-cm$_2$: A record high figure-of-merit of 12.8 GW/cm$_2$. In Proceedings of the 2015 IEEE International Electron Devices Meeting (IEDM), Washington, DC, USA, 7–9 December 2015.
6. Hatakeyama, Y.; Nomoto, K.; Terano, A.; Kaneda, N.; Tsuchiya, T.; Mishima, T.; Nakamura, T. High-breakdown-voltage and low-specific-on-resistance GaN p-n junction diodes on free-standing GaN substrates fabricated through low-damage field-plate process. *Jpn. J. Appl. Phys.* **2013**, *52*, 2441–2452. [CrossRef]
7. Chang, Y.F.; Liao, C.L.; Zheng, B.S.; Liu, J.Z.; Ho, C.L.; Hsieh, K.C.; Wu, M.C. Using two-step mesa to prevent the effects of sidewall defects on the GaN p-i-n diodes. *IEEE J. Quantum Electron.* **2015**, *51*, 8300106. [CrossRef]
8. Carlile, R.N.; Liang, V.C.; Palusinski, O.A.; Smadi, M.M. Trench Etches in Silicon with Controllable Sidewall Angles. *J. Electrochem. Soc.* **1988**, *135*, 2058–2064. [CrossRef]
9. Baliga, B.J. Gallium nitride devices for power electronic applications. *Semicond. Sci. Technol.* **2013**, *28*, 074011. [CrossRef]
10. Rezaei, B.; Asgari, A.; Kalafi, M. Electronic band structure pseudopotential calculation of wurtzite III-nitride materials. *Phys. B Condens. Matter* **2006**, *371*, 107–111. [CrossRef]
11. Mohammad, S.N.; Morkoç, H. Progress and prospects of group-III nitride semiconductors. *Prog. Quantum Electron.* **1996**, *20*, 361–525. [CrossRef]
12. Suzuki, M.; Uenoyama, T.; Yanase, A. First-principles calculations of effective-mass parameters of AlN and GaN. *Phys. Rev. B* **1995**, *52*, 8132. [CrossRef] [PubMed]
13. Santic, B. On the hole effective mass and the free hole statistics in wurtzite GaN. Semicond. *Sci. Technol.* **2003**, *18*, 219.
14. Vurgaftman, I.; Meyer, J.Á.; Ram-Mohan, L.Á. Band parameters for III–V compound semiconductors and their alloys. *J. Appl. Phys.* **2001**, *89*, 5815–5875. [CrossRef]
15. Götz, W.; Johnson, N.; Chen, C.; Liu, H.; Kuo, C.; Imler, W. Activation energies of Si donors in GaN. *Appl. Phys. Lett.* **1996**, *68*, 3144–3146. [CrossRef]
16. Kumar, M.; Bhat, T.N.; Roul, B.; Rajpalke, M.K.; Kalghatgi, A.; Krupanidhi, S. Carrier concentration dependence of donor activation energy in n-type GaN epilayers grown on Si (1 1 1) by plasma-assisted MBE. *Mater. Res. Bull.* **2012**, *47*, 1306–1309. [CrossRef]
17. Podor, B. Thermal ionization energy of Mg acceptors in GaN: Effects of doping level and compensation. In Proceedings of the International Conference on Solid State Crystals 2000: Growth, Characterization, and Applications of Single Crystals, Zakopane, Poland, 9–12 October 2001; Volume 4412, pp. 299–303.
18. Yu, E.; Dang, X.; Asbeck, P.; Lau, S.; Sullivan, G. Spontaneous and piezoelectric polarization effects in III–V nitride heterostructures. *J. Vac. Sci. Technol. B* **1999**, *17*, 1742–1749. [CrossRef]
19. Bernardini, F.; Fiorentini, V.; Vanderbilt, D. Accurate calculation of polarization-related quantities in semiconductors. *Phys. Rev. B* **2011**, *63*, 193201. [CrossRef]
20. Farahmand, M.; Garetto, C.; Bellotti, E.; Brennan, K.F.; Goano, M.; Ghillino, E.; Ghione, G.; Albrecht, J.D.; Ruden, P.P. Monte Carlo simulation of electron transport in the III-nitride wurtzite phase materials system: Binaries and ternaries. *IEEE Trans. Electron Devices* **2001**, *48*, 535–542. [CrossRef]
21. Schwierz, F. An electron mobility model for wurtzite GaN. *Solid State Electron.* **2005**, *49*, 889–895. [CrossRef]
22. Mnatsakanov, T.T.; Levinshtein, M.E.; Pomortseva, L.I.; Yurkov, S.N.; Simin, G.S.; Khan, M.A. Carrier mobility model for GaN. *Solid State Electron.* **2003**, *47*, 111–115. [CrossRef]
23. Sakowski, K.; Marcinkowski, L.; Krukowski, S.; Grzanka, S.; Litwin-Staszewska, E. Simulation of trap-assisted tunneling effect on characteristics of gallium nitride diodes. *J. Appl. Phys.* **2012**, *111*, 123115. [CrossRef]
24. Pearton, S.J.; Abernathy, C.R.; Ren, F. *Gallium Nitride Processing for Electronics, Sensors and Spintronics*; Springer Science Business Media: Berlin, Germany, 2006.
25. Puech, P.; Demangeot, F.; Frandon, J.; Pinquier, C.; Kuball, M.; Domnich, V.; Gogotsi, Y. GaN nanoindentation: A micro-Raman spectroscopy study of local strain fields. *J. Appl. Phys.* **2004**, *96*, 2853. [CrossRef]

26. Chiu, C.H.; Li, Z.Y.; Chao, C.L.; Lo, M.H.; Kuo, H.C.; Yu, P.C.; Lu, T.C.; Wang, S.C.; Lau, K.M.; Cheng, S.J. Efficiency enhancement of UV/blue light emitting diodes via nanoscaled epitaxial lateral overgrowth of GaN on a SiO_2 nanorod-array patterned sapphire substrate. *J. Cryst. Growth* **2008**, *310*, 5170. [CrossRef]
27. Heinke, H.; Kirchner, V.; Einfeldt, S.; Hommel, D. X-ray diffraction analysis of the defect structure in epitaxial GaN. *Appl. Phys. Lett.* **2000**, *77*, 2145. [CrossRef]
28. Dickerson, J.R.; Allerman, A.A.; Bryant, B.N.; Fischer, A.J.; King, M.P.; Moseley, M.W.; Armstrong, A.M.; Kaplar, R.J.; Kizilyalli, I.C.; Aktas, O.; et al. Vertical GaN power diodes with a bilayer edge termination. *IEEE Trans. Electron Devices* **2015**, *63*, 419–425. [CrossRef]
29. Fu, H.; Huang, X.; Chen, H.; Lu, Z.; Zhang, X.; Zhao, Y. Effect of buffer layer design on vertical GaN-on-GaN pn and Schottky power diodes. *IEEE Electron Device Lett.* **2017**, *38*, 763–766. [CrossRef]
30. Hatakeyama, Y.; Nomoto, K.; Kaneda, N.; Kawano, T.; Mishima, T.; Nakamura, T. Over 3.0 GW/cm^2 Figure-of-Merit GaN pn Junction Diodes on Free-Standing GaN Substrates. *IEEE Electron Device Lett.* **2011**, *32*, 1674–1676. [CrossRef]
31. Hu, Z.; Nomoto, K.; Song, B.; Zhu, M.; Qi, M.; Pan, M.; Gao, X.; Protasenko, V.; Jena, D.; Xing, H.G. Near unity ideality factor and Shockley-Read-Hall lifetime in GaN-on-GaN pn diodes with avalanche breakdown. *Appl. Phys. Lett.* **2015**, *107*, 243501. [CrossRef]
32. Monavarian, M.; Pickrell, G.; Aragon, A.A.; Stricklin, I.; Crawford, M.H.; Allerman, A.A.; Celio, K.C.; Léonard, F.; Talin, A.A.; Armstrong, A.M.; et al. 1.1-kV vertical GaN pn diodes with p-GaN regrown by molecular beam epitaxy. *IEEE Electron Device Lett.* **2017**, *38*, 1071–1074.
33. Kizilyalli, I.C.; Edwards, A.P.; Aktas, O.; Prunty, T.; Bour, D. Vertical power pn diodes based on bulk GaN. *IEEE Trans. Electron Devices* **2014**, *62*, 414–422. [CrossRef]
34. Liu, X.; Chiu, H.C.; Wang, H.Y.; Hu, C.; Wang, H.C.; Kao, H.S.; Chien, F.T. 2.4 kV Vertical GaN PN Diodes on Free Standing GaN Wafer Using CMOS-Compatible Contact Materials. *IEEE J. Electron Devices Soc.* **2018**, *6*, 825–829. [CrossRef]
35. Nomoto, K.; Hatakeyama, Y.; Katayose, H.; Kaneda, N.; Mishima, T.; Nakamura, T. Over 1.0 kV GaN p–n junction diodes on free-standing GaN substrates. *Phys. Status Solidi A* **2011**, *208*, 1535–1537. [CrossRef]
36. Yu, C.J.; Lu, J.Y.; Shan, L.W.; Chen, C.J.; Liao, J.H.; Wu, M.C. Over 1 GW/cm2 for high-power GaN pin diodes with edge termination structure and laser annealing. *J. Vac. Sci. Technol. B* **2019**, *37*, 011208. [CrossRef]
37. Zou, X.; Zhang, X.; Lu, X.; Tang, C.W.; Lau, K.M. Fully vertical GaN pin diodes using GaN-on-Si epilayers. *IEEE Electron Device Lett.* **2016**, *37*, 636–639. [CrossRef]